

Thermal states of neutron stars with a consistent model of interior

M. Fortin,¹★ G. Taranto,² G. F. Burgio,² P. Haensel,¹ H.-J. Schulze² and J. L. Zdunik¹

¹ *N. Copernicus Astronomical Center, Polish Academy of Sciences, Bartycka 18, 00-716 Warszawa, Poland*

² *INFN Sezione di Catania, Dipartimento di Fisica, Università di Catania, Via Santa Sofia 64, 95123 Catania, Italy*

Accepted XXX. Received YYY; in original form ZZZ

ABSTRACT

We model the thermal states of both isolated neutron stars and accreting neutron stars in X-ray transients in quiescence and confront them with observations. We use an equation of state and superfluid baryon gaps, which are consistently calculated. We conclude that the direct Urca process is required to be consistent with low-luminous accreting neutron stars. In addition, proton superfluidity and sufficiently weak neutron superfluidity are necessary to explain the cooling of middle-aged neutron stars and to obtain a realistic distribution of neutron star masses.

Key words: stars: neutron – dense matter – equation of state

1 INTRODUCTION

The structure of a neutron star (NS) is determined by the nuclear forces via the equation of state (EOS), which has to be sufficiently stiff in order to support the observed massive $2.0 M_{\odot}$ pulsars (Antoniadis et al. 2013; Fonseca et al. 2016). Nuclear forces determine also the composition of NS cores, as well as the effective masses and superfluid gaps of baryons, and are therefore crucial for the heat capacity and neutrino emission rate in NS cores. These two quantities govern the cooling of middle-aged ($\lesssim 10^5$ yr) isolated NS (INS) and are also involved in the determination of the surface photon luminosity of accreting NS in X-ray transients in quiescence (qXRT) (Yakovlev & Pethick 2004).

Theoretical calculations of these basic properties of NS matter are difficult and suffer from big uncertainties, stemming from the deficiencies and approximations in the many-body theory of baryonic matter, and the lack of knowledge of strong interactions at high density (many-body forces, effect of the quark structure of baryons, etc., see, e.g., Haensel et al. 2007a). It seems thus reasonable to consider first the simplest (minimal) model of NS with nucleon cores, consisting of highly asymmetric nuclear matter permeated by a degenerate quasi-free Fermi gas of electrons, and above the muon threshold, also muons. In the minimal model, nucleons are treated as point-like, and interact via a two-body potential and three-body forces. The solution to the many-body problem is to be consistent with laboratory nuclear data, referring mainly to weakly asymmetric nuclear matter and density close to normal nuclear density $n_0 = 0.16 \text{ fm}^{-3}$. Even for this model, however, application to NS cores involves a huge extrapolation to $(6 - 8)n_0$, at very large neutron excess.

Fortunately, high-density NS models can be confronted with astrophysical data: measurements of NS masses and radii (Özel & Freire 2016; Lattimer 2012; Haensel et al. 2016), surface tem-

perature for INS of known or estimated age, and thermal photon luminosity of qXRT with an estimated time-averaged accretion rate onto the NS (see Beznogov & Yakovlev 2015a for recent observational data). This can hopefully help in unveiling the real physics of the NS core and thus testing microscopic calculations starting from nuclear forces.

Recently, initial stages of such a program were carried out in Baldo et al. (2014); Sharma et al. (2015); Taranto et al. (2016). The starting point was the AV18 two-body potential plus an Urbana model of three-body interaction, and the many-body theory was the Brueckner-Hartree-Fock (BHF) approximation. The three-body interaction in nuclear matter was adjusted to nuclear saturation data, and required to be consistent with the phenomenology of heavy ion collisions and basic NS data (Taranto et al. 2013). The model has at the saturation point a symmetry energy of 32 MeV and a slope of 53 MeV, which is in agreement with current nuclear constraints, see, e.g., Figure 13 in Fortin et al. (2016).

Then a unified EOS valid for the outer crust, inner crust, and the core was calculated (Sharma et al. 2015), nucleon effective masses were obtained, and neutrino emissivities (assuming normal nucleons) calculated (Baldo et al. 2014). Finally, superfluid gaps for neutrons and protons for the same nucleon interaction were obtained and used to model the cooling Cas A NS and the thermal states of middle-aged, $\sim (10^2 - 10^6)$ yr, INS (Taranto et al. 2016).

An important feature of the latter reference was the fact that the BHF EOS allows for the very efficient direct Urca (DU) cooling process to set in at a fairly low baryon density $n_B = 0.44 \text{ fm}^{-3}$ (proton fraction $x_p = 0.136$), corresponding to a NS mass of $1.1 M_{\odot}$ (Taranto et al. 2016), in contrast to most other comparable studies in the literature (Gusakov et al. 2005; Page et al. 2011; Yakovlev et al. 2011; Shternin et al. 2011; Blaschke et al. 2012, 2013; Fortin et al. 2016), which employ smaller nuclear symmetry energies and later onset of the DU process. Non-millisecond pulsars, which were not recycled and thus have a mass near their birth mass, have masses as low as $\sim (1.1 - 1.2) M_{\odot}$ (Özel & Freire 2016; Lattimer 2012).

★ E-mail: fortin@camk.edu.pl

which is close to the theoretical minimum NS mass due to thermal evolution (Yakovlev & Pethick 2004; Page 2009; Burgio et al. 2011). Thus with the EOS used in this work, the DU process is operating in all currently observed NS.

Nevertheless in Taranto et al. (2016) a very satisfactory reproduction of all current NS cooling data could be obtained for a certain choice of pairing gaps.

In the present paper we extend the theoretical study of cooling middle-aged INS initiated in Taranto et al. (2016) to the case of qXRT, old NS of age $\sim (10^8 - 10^9)$ yr that accrete matter from their companion star during short periods of time resulting in the heating of their interior. Theoretical models for INS are represented by *cooling curves* relating the effective surface temperature to the NS age. A cooling curve corresponds to an assumed NS mass and composition of the heat-blanketing envelope. For qXRT sources theory yields instead *heating curves* showing photon luminosity versus time-averaged accretion rate (Yakovlev & Pethick 2004). A heating curve is obtained for a given NS mass, assumed composition of heat blanketing envelope, and value of the total deep crustal heating per one accreted nucleon.

The article is organized as follows. The microscopic model of NS interior is presented in Sect. 2. The approach to the modelling of the thermal evolution and of the stationary states of transiently accreting NS is described in Sect. 3. Theoretical predictions for INS and qXRT are presented in Sect. 4. Comparison with measurements of surface thermal luminosity for middle-aged INS and of qXRT are used to test the validity of the microscopic model and to select an optimal model for the superfluid properties in the NS core consistent with all the available observational data. Sect. 5 summarizes our results and draws the conclusions.

2 MICROSCOPIC MODEL

2.1 EOS and composition of the core

We calculate the EOS of nuclear matter within the BHF theoretical approach (Baldo 1999). The starting point is the Brueckner-Bethe-Goldstone (BBG) equation for the in-medium G -matrix, whose only input is the nucleon-nucleon (NN) bare potential V ,

$$G[n_B; \omega] = V + \sum_{k_a k_b} V \frac{|k_a k_b \mathcal{Q}(k_a k_b)|}{\omega - e(k_a) - e(k_b)} G[n_B; \omega], \quad (1)$$

where $n_B = \sum_{k < k_F}$ is the nucleon number density, ω is the starting energy, and the Pauli operator \mathcal{Q} determines the propagation of intermediate baryon pairs. The single-particle (s.p.) energy reads

$$e(k) = e(k; n_B) = \frac{k^2}{2m} + U(k; n_B), \quad (2)$$

where the s.p. potential $U(k; n_B)$ is calculated in the so-called *continuous choice* and is given by

$$U(k; n_B) = \text{Re} \sum_{k' < k_F} \langle k k' | G[n_B; e(k) + e(k')] | k k' \rangle_a, \quad (3)$$

where the subscript a indicates antisymmetrization of the matrix element. Finally the energy per nucleon is expressed by

$$\frac{E}{A} = \frac{3}{5} \frac{k_F^2}{2m} + \frac{1}{2n_B} \sum_{k < k_F} U(k; n_B). \quad (4)$$

In this scheme, we use the Argonne V_{18} potential (Wiringa et al. 1995) as bare NN interaction V in the BBG equation (1), supplemented by a suitable three-nucleon force (TBF) introduced

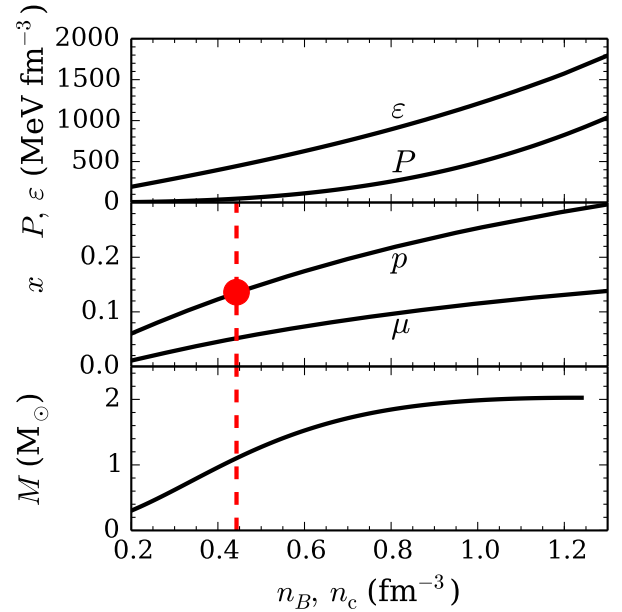


Figure 1. (Color online) Pressure and energy density (a), and proton and muon fractions (b) are plotted as functions of baryon number density n_B in beta-stable matter for the BHF EOS. In the lower panel (c) the neutron star mass is shown as functions of the central density n_c . The DU onset is indicated by the red dotted line.

in order to reproduce correctly the nuclear matter saturation point. In this work we adopt the phenomenological Urbana-type UIX TBF (Carlson et al. 1983; Schiavilla et al. 1986; Pudliner et al. 1997; Li et al. 2008) as input, which consists of an attractive term due to two-pion exchange with excitation of an intermediate Δ resonance, and a repulsive phenomenological central term.

Further important ingredients in the cooling simulations are the neutron and proton effective masses,

$$\frac{m^*(k)}{m} = \frac{k}{m} \left[\frac{de(k)}{dk} \right]^{-1}, \quad (5)$$

which we derive consistently from the BHF s.p. energy $e(k)$, Eq. (2), see Ref. (Baldo et al. 2014) for the numerical parametrizations. Though their effect is not large compared to other uncertainties regarding the cooling, we like to stress that in this paper a consistent treatment is used.

In Fig. 1 we display the NS EOS obtained with the BHF model for beta-stable and charge-neutral matter. The upper panel shows pressure and energy density as functions of the baryon density, whereas the middle panel shows proton and muon fractions. The vertical red dotted line indicates the value of the density threshold at which the DU process sets in, i.e. $n_B = 0.44 \text{ fm}^{-3}$, where $x_p = 0.136$. In the lower panel we show the NS mass vs. central density relation, obtained by solving the standard Tolman-Oppenheimer-Volkov equations for the NS structure. We notice that the BHF model reaches a maximum mass slightly above two solar masses $M_{\text{max}} = 2.01 M_{\odot}$, and thus is compatible with recent NS observations (Antoniadis et al. 2013; Fonseca et al. 2016), and that the DU process can potentially operate in nearly all stars, $M/M_{\odot} > 1.10$.

This latter feature deserves a comment. As was already mentioned, our BHF calculations reproduce the empirical saturation parameters of nuclear matter. A relatively strong growth of the symmetry energy at supranuclear densities, and the associated relatively low DU threshold density, result from our microscopic calculations,

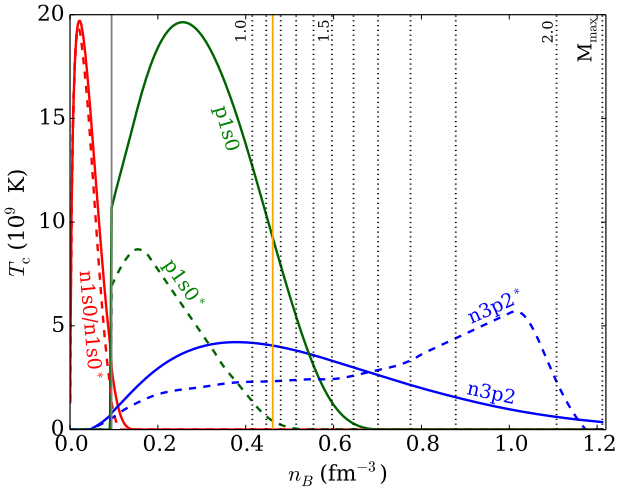


Figure 2. (Color online) Critical temperatures in NS matter for the BHF model in the n1S0, p1S0 and n3P2 channels, including (*) or not effective mass effects. The vertical dotted lines indicate the central density of NS with different masses $M/M_\odot = 1.0, \dots, 2.0$, up to the maximum mass value. DU onset occurs at the vertical solid (yellow) line (see section 3.2).

and we had no freedom to modify these quantities within our approach.

2.2 Pairing gaps

An essential ingredient for cooling simulations is the knowledge of the 1S0 and 3P2 pairing gaps for neutrons and protons in beta-stable matter, which on one hand block neutrino processes and on the other hand open new ones (see Section 3.2) (Yakovlev et al. 2001). In this paper we present calculations obtained using gaps computed consistently with the EOS, i.e., based on the same NN interaction and using the same medium effects (TBF and effective masses), as shown in Zhou et al. (2004). To be more precise, and focusing on the more general case of pairing in the coupled 3P2 channel, the pairing gaps were computed on the BCS level by solving the (angle-averaged) gap equation (Amundsen & Østgaard 1985; Baldo et al. 1992; Takatsuka & Tamagaki 1993; Elgarøy et al. 1996; Khodel et al. 1998; Baldo et al. 1998) for the two-component $L = 1, 3$ gap function,

$$\begin{pmatrix} \Delta_1 \\ \Delta_3 \end{pmatrix}(k) = -\frac{1}{\pi} \int_0^\infty dk' k'^2 \frac{1}{E(k')} \begin{pmatrix} V_{11} & V_{13} \\ V_{31} & V_{33} \end{pmatrix}(k, k') \begin{pmatrix} \Delta_1 \\ \Delta_3 \end{pmatrix}(k') \quad (6)$$

with

$$E(k)^2 = [e(k) - \mu]^2 + \Delta_1(k)^2 + \Delta_3(k)^2, \quad (7)$$

while fixing the (neutron or proton) density,

$$n = \frac{k_F^3}{3\pi^2} = 2 \sum_k \frac{1}{2} \left[1 - \frac{e(k) - \mu}{E(k)} \right]. \quad (8)$$

Here $e(k)$ are the BHF s.p. energies, Eq. (2), containing contributions due to two-body and three-body forces, $\mu \approx e(k_F)$ is the chemical potential determined self-consistently from Eqs. (6–8), and

$$V_{LL'}(k, k') = \int_0^\infty dr r^2 j_{L'}(k'r) V_{LL'}^{TS}(r) j_L(kr) \quad (9)$$

are the relevant potential matrix elements ($T = 1$ and $S = 1$; $L, L' = 1, 3$ for the 3P2 channel, $S = 0$; $L, L' = 0$ for the 1S0 channel) with

$$V = V_{18} + \bar{V}_{\text{UIX}}. \quad (10)$$

composed of two-body force and averaged TBF. The relation between (angle-averaged) pairing gap at zero temperature $\Delta \equiv \sqrt{\Delta_1^2(k_F) + \Delta_3^2(k_F)}$ obtained in this way and the critical temperature of superfluidity is then $T_c \approx 0.567\Delta$.

Fig. 2 displays the various pairing gaps as a function of baryonic density of beta-stable matter for the BHF model. In this way one can easily identify which range of gaps is active in different stars, whose central densities are shown by vertical dotted lines for given NS mass. We stress that in Zhou et al. (2004) no polarization corrections (Lombardo & Schulze 2001; Baldo & Schulze 2007; Gandolfi et al. 2008; Ding et al. 2016) were taken into account, which for the 1S0 channel are known to be repulsive, but for the 3P2 are still essentially unknown; and this might change the value of these gaps even by orders of magnitude (Khodel et al. 2004; Schwenk & Friman 2004; Ding et al. 2016).

In order to represent this uncertainty, in the cooling simulations performed in Taranto et al. (2016) we used the density dependence of the pairing gaps shown in Fig. 2, but employing global scaling factors s_p and s_n for the p1S0 and n3P2 gaps, respectively. One should notice that the n3P2 gaps shown in the figure are larger than those currently employed in cooling simulations, and that at the moment there exists no satisfactory theoretical calculation of p-wave pairing that includes consistently all medium effects.

2.3 Models of the crusts

The structure of the NS crust depends on its formation scenario (Haensel & Zdunik 1990a; Zdunik & Haensel 2011). Consider first an isolated NS born in a core-collapse supernova explosion. Then the crust is formed during the cooling of the very hot and fully fluid proto-NS. In the initial state, the composition of the outer layer corresponds to nuclear equilibrium, because $T > 10^{10}$ K and therefore nuclear reactions are sufficiently rapid. The hot plasma crystallizes in the process of cooling. A standard assumption is that during the process of cooling and crystallization the plasma keeps the nuclear equilibrium. Consequently, when matter becomes strongly degenerate, the structure and EOS of the crust can be well approximated by *cold catalyzed matter* - the ground state (GS) of the matter at $T = 0$. The structure of the GS crust is calculated using the energy density functional (EDF) based on the microscopic BHF theory of nuclear matter, applied previously for the NS core. In this way we maintain a unified description of the whole NS interior based on a microscopic theory of nuclear matter (Sharma et al. 2015).

The GS approximation is not valid for NS in qXRT. Such NS formed their crust by accreting plasma from their companion star in a low-mass X-ray binary. The matter accreted onto the NS surface during ($10^8 - 10^9$) yr compresses and pushes down the original pre-accretion crust. During the active stages of a XRT the outermost layer of accreted plasma undergoes thermonuclear flashes, observed as X-ray bursts, but the layers deeper than a few meters have $T < 5 \times 10^8$ K and therefore cannot keep nuclear equilibrium during compression. On the contrary, with increasing depth and density, the composition of the matter diverges from nuclear equilibrium, because the temperature is too low for the thermonuclear fusion to proceed: the fusion reactions are blocked by Coulomb barriers. Consequently, the only nuclear reactions are electron captures and neutron emissions and absorptions induced by compression.

Due to electron captures the neutron excess in nuclei increases with increasing density, and finally neutrons start to drip out from

nuclei. The neutron drip is triggered by the electron capture; for our specific model this occurs at $6 \times 10^{11} \text{ g cm}^{-3}$, which is similar to the neutron drip density in the GS crust. With increasing density, electron captures trigger further neutron emission, so that the mass number of nuclei decreases, and they become more and more neutron rich. Then, at densities greater than $10^{12} \text{ g cm}^{-3}$ the proton number in the nuclei becomes so low ($Z \sim 10$) that pycnonuclear fusion of two neighboring nuclei due to the (growing with density) zero-point motion of nuclei around their lattice sites becomes possible on a timescale shorter than the compression time. This leads to the further neutronization of the crust matter. Eventually, all the pre-accretion crust dissolves in the liquid core, and a fully-accreted crust is formed. Then, the layered structure of the crust ceases to evolve and becomes quasistationary, with matter elements moving inwards due to compression and undergoing exothermic nuclear transformations.

The total heat release is calculated using a microscopic model of the dense degenerate plasma, and by following the nuclear evolution of an element of matter consisting initially of X-ray ashes, under quasistatic compression from 10^7 g cm^{-3} to $10^{14} \text{ g cm}^{-3}$ (crust-core interface). The microscopic model for a fully accreted crust is taken from [Haensel & Zdunik \(2008\)](#), which calculated the EOS and distribution of deep crustal heating sources. It is assumed that the X-ray bursts ashes consist of $A = 56$ nuclei. Note that the distribution of deep heating sources does not influence the stationary thermal state of qXRT, and only the total heat release is important. The total deep crustal heating per one accreted nucleon is in our case $Q_{\text{DCH}} = 1.9 \text{ MeV}$ ([Haensel & Zdunik 2003](#)).

3 THERMAL EVOLUTION OF INS AND QXRT

3.1 Thermal evolution of a INS

Let us start by sketching the thermal evolution of a INS (see [Yakovlev & Pethick 2004](#); [Page 2009](#) for a detailed review). A proto-neutron star is formed in a supernova event with a high temperature $T \sim 10^{11} \text{ K}$. The proto-neutron star becomes a NS when it gets transparent to the neutrinos that are formed in its interior. During ~ 100 years, the crust stays hot due to its low thermal conductivity, while the core cools by emission of neutrinos. Therefore, the core and the crust cool independently and the evolution of the surface temperature reflects the thermal state of the crust and is sensitive to its physical properties (see, e.g., [Fortin et al. 2010](#) and references therein). Then the core and the crust thermal evolutions couple. The cooling wave from the core reaches the surface and the whole NS cools by the emission of neutrinos, mainly from the core. This is the neutrino cooling stage. The evolution of the surface temperature depends mainly on the physical properties of the core. As the temperature in the interior of the NS continues to decrease, the neutrino luminosity becomes comparable to the photon luminosity. The NS then enters the photon cooling stage and the evolution of the internal temperature is governed by the emission of photons from the surface and is sensitive to the properties of the outer parts of the star.

Currently, all INS for which the surface temperature has been measured thanks to X-ray observations are at least ~ 300 years old and they are all in the neutrino- and photon-cooling stages (see, e.g., Table 1 in [Beznogov & Yakovlev 2015a](#)). Therefore they have an isothermal interior, i.e., the redshifted internal temperature $T_i(t) = T(t, r)e^{\phi(r)}$ is constant throughout the interior for densities larger than $\rho_B \simeq 10^{10} \text{ g cm}^{-3}$. Here $T(r, t)$ is the local temperature

and $e^{\phi(r)}$ the metric function. Thus the heat equation reads:

$$C(T_i) \frac{dT_i}{dt} = -L_\nu^\infty(T_i) - L_\gamma^\infty(T_s). \quad (11)$$

In this equation $T_s(t)$ is the effective surface temperature and the relation $T_s(T_i)$ is determined by the model of the heat blanketing envelope (see hereinafter). $C(T_i)$ is the total specific heat integrated over the whole star and the quantities L_ν^∞ , L_γ^∞ are respectively the redshifted total neutrino luminosity and the surface photon luminosity detected by an observer at infinity:

$$L_\nu^\infty(T_i) = 4\pi \int_0^R dr r^2 e^{2\phi} Q_\nu / \sqrt{1 - 2GM/r}, \quad (12)$$

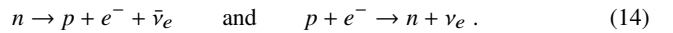
$$L_\gamma^\infty(T_s) = 4\pi R^2 \sigma_{\text{SB}} T_s^4 (1 - 2GM/R), \quad (13)$$

with σ_{SB} being the Stefan-Boltzmann constant, Q_ν the neutrino emissivity, $m(r)$ the gravitational mass enclosed in a sphere of radius r , and $M = m(R)$ the gravitational mass of the star of radius R . The temperature measured by an observer at infinity is then $T_s^\infty = e^{\phi(R)} T_s = T_s \sqrt{1 - 2GM/R}$.

3.2 Microphysical ingredients

The main contribution to the total specific heat $C(T_i)$ comes from the NS core, i.e., from the neutrons, protons and electrons. If the core is non-superfluid, most of the specific heat comes from the neutrons. If the neutrons and protons are superfluid, then below their superfluid critical temperature T_c their contributions become exponentially suppressed and C is dominated by the electrons.

Let us now review the various contributions to the neutrino emissivity in the NS core, which dominates the total neutrino luminosity L_ν^∞ . In a non-superfluid NS the most powerful neutrino process is the so-called direct Urca (DU) process, which is in fact the neutron β -decay followed by its inverse reaction:



For this process, the neutrino emissivity varies as T^6 . However, the energy and momentum conservation imposes a density threshold to this process ([Lattimer et al. 1991](#)). For the EOS used in this work the DU process sets in at $n_{\text{B}}^{\text{DU}} = 0.44 \text{ fm}^{-3}$, where the proton fraction $x_p = 0.136$, as indicated by the vertical red dotted line in [Fig. 1](#), and thus the DU process operates in the central part of NS with masses larger than $M_{\text{DU}} = 1.10 M_\odot$, corresponding to the yellow vertical solid line in [Fig. 2](#).

Various less efficient neutrino processes may be operating in the NS core (see [Yakovlev et al. 2001](#) for a review) and dominate when the DU process is forbidden or strongly reduced. The two main ones with an emissivity $Q_\nu \propto T^8$ are:

- the so-called modified Urca (MU) process:



where N is a spectator nucleon that ensures momentum conservation. Nevertheless, since five degenerate fermions are involved instead of three, the efficiency is significantly reduced as compared with the DU process.

- the nucleon-nucleon bremsstrahlung:



with N a nucleon and ν , $\bar{\nu}$ an (anti)neutrino of any flavor.

The effect of the neutron or proton superfluidity on the neutrino emissivity is twofold. On one hand, when the temperature decreases

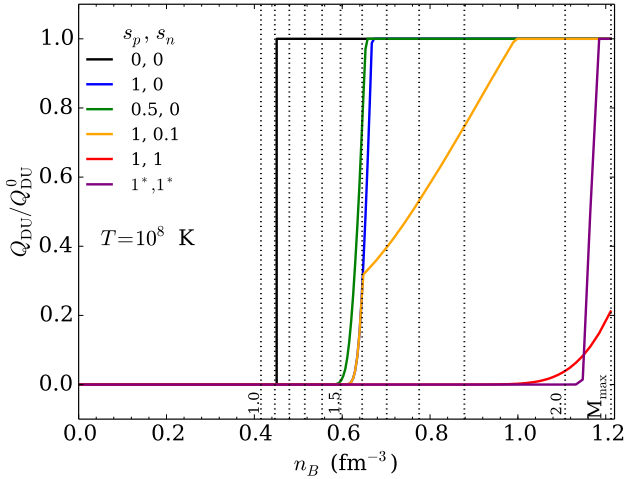


Figure 3. (Color online) DU ratio: DU emissivity Q_{DU} for different superfluid models (s_p, s_n) over DU emissivity Q_{DU}^0 for non-superfluid matter, at $T = 10^8$ K. The vertical dotted lines indicate the central density of NS with different masses $M/M_\odot = 1.0, 1.1, \dots, 2.0$, up to $M_{\text{max}} = 2.01 M_\odot$.

below the critical superfluid temperature of a given type of baryons, the neutrino emissivity of processes involving a superfluid baryon is exponentially reduced. For example, proton superfluidity in the core of a NS suppresses both Urca processes (DU and MU) but does not affect the neutron-neutron bremsstrahlung.

Fig. 3 shows, as a function of the baryon number density of NS matter, the ratio of the emissivity of the DU process for various superfluid models over the DU emissivity in non-superfluid matter, Q_{DU}^0 , for a temperature $T = 10^8$ K. For densities lower than the onset density $n_B^{\text{DU}} = 0.44 \text{ fm}^{-3}$, or equivalently masses smaller than $M_{\text{DU}} = 1.1 M_\odot$ the ratio is set to zero and the DU process can not operate at the center of the star. In the case of non-superfluid matter (black curve), the ratio for $n_B > n_B^{\text{DU}}$ (or at the center of stars with $M > M_{\text{DU}}$) is by definition equal to 1 and the DU process is fully operative in the central part of the NS.

Let us now turn on the proton superfluid without effective mass effect, but not the neutron one; this case corresponds to $s_p = 1$ and $s_n = 0$ (blue curve). The proton critical temperature T_c^p is smaller than $T = 10^8$ K for densities larger than $n_B^p(1,0) = 0.67 \text{ fm}^{-3}$, or masses above $M^p(1,0) = 1.65 M_\odot$. Hence the DU emissivity is not affected by the superfluidity for such densities and in the center of NS with such masses, and the DU ratio is equal to 1. For $n_B^{\text{DU}} < n_B < n_B^p(1,0)$ or equivalently $M_{\text{DU}} < M < M^p(1,0)$ however, the DU process is allowed and the protons are superfluid at $T = 10^8$ K. These being involved in the reaction in Eq. (14), the DU emissivity and thus the ratio is exponentially reduced. Consequently the DU ratio is no longer a step-like function, but a smooth function of the density or the NS mass: the DU process is turned off below M_{DU} , is equal to the one of non-superfluid matter at the center of NS with masses bigger than $M^p(1,0)$, above which the protons are no longer superfluid, and is reduced due to superfluid effects in between the two boundaries.

The superfluid effects are similar if we now artificially divide the proton critical temperature by a factor of 2, while keeping the neutrons non-superfluid, ($s_p = 0.5, s_n = 0$, green curve). Only the density and mass at which $T_c^p < 10^8$ K differ: $n_B^p(0.5,0) = 0.66 \text{ fm}^{-3}$, $M^p(0.5,0) = 1.63 M_\odot$.

Let us now consider superfluid protons (with no scaling) and scale the neutron superfluidity by a factor 0.1 ($s_p = 1, s_n = 0.1$,

yellow curve). Then the density for which the proton critical temperature is smaller than 10^8 K is $n_B^p(1,0.1) = n_B^p(1,0)$, hence $M^p(1,0.1) = M^p(1,0)$, and for the neutron $n_B^n(1,0.1) = 1.0 \text{ fm}^{-3}$, which is larger than $n_B^p(1,0.1)$ ($M^n(1,0.1) = 1.97 M_\odot$). If two species involved in the DU process are superfluid, then the exponential reduction is roughly speaking dominated by the stronger superfluidity (Yakovlev et al. 2001), in this case the proton one. Consequently for $n_B^{\text{DU}} < n_B < n_B^p(1,0.1)$ the ratio is similar as for the case $s_p = 1$ and $s_n = 0$. Then for $n_B^p(1,0.1) < n_B < n_B^n(1,0.1)$ the DU process is not suppressed because of the proton superfluidity, but because of the neutron one. Hence the ratio is still smaller than 1. Finally when $n_B > n_B^n(1,0.1)$, the DU process is not affected anymore and the ratio equal to 1.

If we now consider the two unscaled models for the proton and neutron superfluidity without medium effects (i.e., $m_i^* = m_i$), $s_p = 1$ and $s_n = 1$ (red curve), the neutron critical temperature remains larger than 10^8 K up to densities comparable to the central density of the NS with the maximum mass $n_B^c(M_{\text{max}})$. Thus the DU process is strongly reduced because of the proton and neutron superfluidity and the DU ratio is much smaller than 1 for any NS mass. Similar observations can be made for the case of the proton and neutron superfluidities including the effective mass effects (m_i replaced by m_i^*), $s_p = 1^*$ and $s_n = 1^*$ (darkred curve), except that neither the protons nor the neutrons are superfluid above $n_B^p(1^*,1^*) = 1.19 \text{ fm}^{-3}$, $M^p(1^*,1^*) = 2.005 M_\odot$, and thus the ratio is equal to 1.

On the other hand, the pairing of baryons initiates a new type of neutrino processes called the pair breaking and formation (PBF) processes. The energy is released in the form of a neutrino-antineutrino pair when a Cooper pair of baryons is formed. The process starts when $T < T_c$, is maximally efficient when $T \sim 0.8 T_c$, and is exponentially suppressed for $T \ll T_c$ (Yakovlev et al. 2001). For both 1S0 and 3P2 pairings, the emission of neutrinos by the PBF process can occur through two different channels: the axial and vector channels (Page 2009). Since the vector part of the PBF process is strongly suppressed (Leinson & Pérez 2006a,b), the axial part is in fact the main contributor to the PBF neutrino emissivity. In addition, as pointed out recently in Leinson (2016) and references therein: (a) for the 1S0 pairing of baryons, in our case for the protons in the core, the neutrino losses in the axial channel are very small and can be neglected in the calculations; (b) for the n3P2 pairing in the core, taking into account the anomalous contributions in the axial channel leads to an emissivity four times smaller than the one used in previous works, e.g., in Page et al. (2009); Taranto et al. (2016).

Yet, as the n3P2 gap extends up to very large density, see Fig. 2, superfluidity provides an efficient means to block the DU cooling process, in particular the n3P2* model taking into account medium effects. The price to pay is an enhanced PBF cooling rate close to the critical temperature in that case. Also the p1S0 gap might persist throughout NS up to about $1.6 M_\odot$ (for pure BCS gaps), and at this threshold the DU process will invariably set in and cool the heavier stars very rapidly, if neutrons are not superfluid.

3.3 Heat-blanketing envelope

In a few hundred years the redshifted temperature inside a newly born NS for density larger than $\rho_b \simeq 10^{10} \text{ g cm}^{-3}$ becomes uniform due to the high thermal conductivity. However, in the NS atmosphere the heat transport is dominated by the photons and in between there exists a thin layer, which has a low thermal conductivity, since the

electrons are not highly degenerate and the high density strongly prevents photon transport. This results in high temperature gradients in the envelope, that is few hundred meters thick.

Therefore, a variety of models are devoted solely to the precise modeling of the heat-blanketing envelope, in the plane-parallel and stationary approximation, resulting in a relation between the surface temperature T_s and the temperature T_i at ρ_b . Some models consider various compositions for the envelope and in particular, different abundances of light elements such as hydrogen, helium, carbon resulting from the accretion of matter (Potekhin et al. 1997) or binary mixtures of these (Beznogov et al. 2016). The higher the abundances of light elements, the higher the surface temperature for a given T_i . As these abundances are unknown for a given NS, we will consider in the following two limiting cases corresponding to the absence of light elements (non-accreted envelope) and a maximum amount of them (fully accreted envelope), and use the non-magnetic models from Potekhin et al. (2003).

3.4 Thermal evolution of qXRT

qXRT contain NS in binary systems, which accrete matter from a companion star during short active phases with a high luminosity followed by long period of quiescence with zero or strongly reduced accretion and low luminosity. Here, we will model the quiescent phase. The accreted matter sinks gradually in the interior of the NS and undergoes a series of nuclear reactions (beta captures, neutron absorption and emission and pycnonuclear fusions). These reactions release some heat, $Q_{\text{DCH}} \sim 2 \text{ MeV}$ per accreted nucleon, which propagates into the whole NS, inwards heating the core and outwards emitted in the form of photons at the surface. This is the so-called deep crustal heating. A state of thermal equilibrium with a constant T_i throughout the star is reached in $\sim 10^5$ years as the episodes of heating due to the accretion followed by quiescence and cooling through the emission of neutrinos proceed (Yakovlev et al. 2003, 2004). The internal temperature T_i of such a star is then determined by the following equation:

$$L_{\text{DCH}}^{\infty}(\dot{M}) = L_{\nu}^{\infty}(T_i) + L_{\gamma}^{\infty}(T_s) \quad (17)$$

with L_{ν}^{∞} and L_{γ}^{∞} being the neutrino and photon luminosities described before. The deep crustal heating power L_{DCH}^{∞} is given by:

$$L_{\text{DCH}}^{\infty}(\dot{M}) = e^{\phi} \frac{Q_{\text{DCH}}}{m_{\text{N}}} \dot{M} \quad (18)$$

with m_{N} the atomic mass unit and \dot{M} the mean accretion rate, assumed to be constant, averaged over periods of accretion and quiescence.

3.5 Cooling and heating curves

In the following we make use of the one-dimensional code called NSCool¹ based on an implicit scheme developed by Henyey et al. (1964), suitable for the study of spherically symmetric problems, that employs the Newton-Raphson method to solve the heat equation. We then obtain for a NS of given mass and composition of the envelope so-called *cooling curves* of INS showing equivalently L_{γ}^{∞} as a function of the NS age t , and *heating curves* of qXRT relating the L_{γ}^{∞} in quiescence to the estimated time-averaged accretion rate

\dot{M} (Yakovlev et al. 2003). We will compute such cooling and heating curves for various superfluid models using the gaps calculated with the same nuclear interaction model as the EOS.

Note that we do not include the effect of the magnetic field B on the thermal evolution and on the thermal transport in the envelope (Potekhin et al. 2003). On one hand the magnetic field is likely to affect the cooling of INS (see, e.g., Aguilera et al. 2008; Pons et al. 2009), as it is estimated that they have $B \gtrsim 10^{12} \text{ G}$; however this is beyond the scope of the present paper. On the other hand, for qXRT its influence on cooling and heating can be neglected as these objects have $B \simeq (10^8 - 10^9) \text{ G}$ as a result of the accretion-induced decay of the magnetic field.

4 RESULTS

4.1 Non-superfluid matter

Let us first consider the thermal states of INS and qXRT for the case of non-superfluid matter, i.e., for $s_p = 0$, $s_n = 0$, presented in Fig. 4. Cooling and heating curves are calculated for masses ranging from $1.0 M_{\odot}$ to $M = M_{\text{max}}$ for two limiting models of atmosphere (non-accreted in blue and fully accreted in red). Observational data for INS and qXRT from Beznogov & Yakovlev (2015a) and references therein are also plotted.

However, as noted in the same reference, it should be pointed out that in many cases the distance to the object, the composition of its atmosphere, thus its luminosity, and its age or average accretion rate are rather estimated than measured. Thus in these cases, we use large error bars (a factor 0.5 and 2) to reflect this uncertainty and do not intend to constrain the mass of any object. We point out that we do not model the thermal evolution of the CasA NS, as it was already performed in Taranto et al. (2016). Note that the direct observation of its cooling is questioned, see Posselt et al. (2013); Elshamouty et al. (2013), but also Ho et al. (2015). Two objects are particularly constraining: 1) XMMU J1731–347 (Klochov et al. 2015), a middle-aged and yet very hot INS, number 8 in Fig. 4 left, shown to have a carbon atmosphere and whose mass has been constrained to be larger than $1.4 M_{\odot}$ (Ofengeim et al. 2015), but see the discussion about the limitations of this result in the reference; 2) SAX J1808–3658 (Heinke et al. 2009), a low-luminosity qXRT with a well-constrained accretion rate, number 5 in Fig. 4 right, which has been shown to have a relatively low mass $M \lesssim 1.7 M_{\odot}$ by modeling its pulse shapes observed in X-ray (Morsink & Leahy 2011).

In a NS with $M < M_{\text{DU}}$, the DU process is turned off and consequently the total neutrino emissivity is orders of magnitude smaller than for a NS with a mass above the DU threshold. Consequently the former has at a given age or accretion rate a higher luminosity than the latter. Note that on one hand all NS with $M < M_{\text{DU}}$ have a small neutrino emissivity, hence their cooling and heating curves are nearly indistinguishable on the scale of Fig. 4. On the other hand, for objects with $M > M_{\text{DU}}$, the larger is the mass and thus the bigger is the central region of the star where the DU process operates, the lower is the luminosity and the cooling/heating curves are no longer superimposed. This behavior can clearly be seen in Fig 4, where cooling and heating curves are plotted for various masses.

Comparing the influence of the envelope model on INS, for a given age in the neutrino-cooling stage, a model obtained for a fully-accreted one has a higher luminosity than one with a non-accreted envelope. This originates from the fact that envelopes with

¹ freely available online: <http://www.astroscu.unam.mx/neutrones/NSCool/>

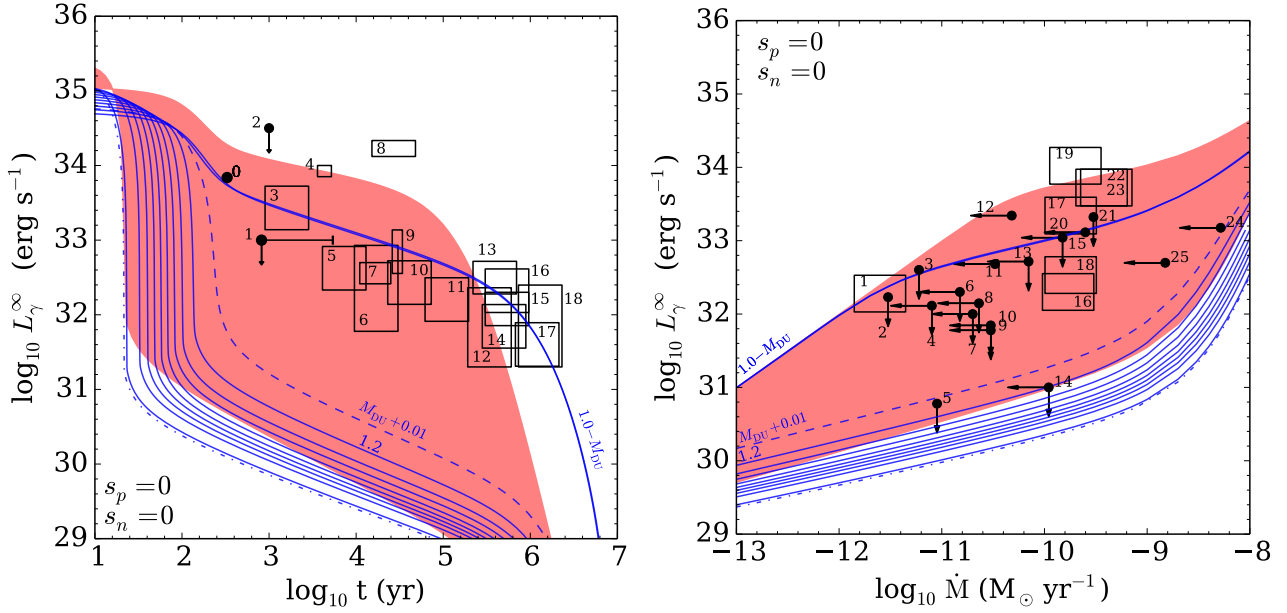


Figure 4. Thermal states of INS (left) and qXRT (right) for non-superfluid matter ($s_p = 0$, $s_n = 0$). For a non-accreted (Fe) envelope, thermal states are plotted in blue for $M/M_\odot = 1.0, 1.1, 1.2, \dots, 2$ (solid lines), for $M = M_{\max}$ (dot-dashed line) and $M = M_{\text{DU}} + 0.01 M_\odot = 1.11 M_\odot$ (dashed). For a fully-accreted envelope, the red contour corresponds to the area covered by the thermal states for $1.0 M_\odot < M < M_{\max}$.

Observational data for INS: 0 - CasA NS, 1 - PSR J0205+6449 (in 3C58), 2 - PSR B0531+21 (Crab), 3 - PSR J1119-6127, 4 - RX J0822-4300 (in PupA), 5 - PSR J1357-6429, 6 - PSR B1706-44, 7 - PSR B0833-45 (Vela), 8 - XMMU J1731-347, 9 - PSR J0538+2817, 10 - PSR B2334+61, 11 - PSR B0656+14, 12 - PSR B0633+1748 (Geminga), 13 - PSR J1741-2054, 14 - RX J1856.4-3754, 15 - PSR J0357+3205 (Morla), 16 - PSR B1055-52, 17 - PSR J2043+2740, 18 - RX J0720.4-3125.

For qXRT: 1 - IGR 00291+5934, 2 - XTE J1814-338, 3 - XTE J1751-305, 4 - XTE J1807-294, 5 - SAX J1808-3658, 6 - SAX J18104-2609, 7 - XTE J0929-314, 8 - XTE 2123-058, 9 - NGC6440 X2, 10 - EXO 17474-214, 11 - Cen X-4, 12 - 4U1730-22, 13 - 2S1803-245, 14 - 1H 1905+000, 15 - Terzan 1, 16 - MXB 1659-29, 17 - RX J1709-2639, 18 - NGC 6440 X1, 19 - SAX J1750.8-2900, 20 - 1M 1716-315, 21 - Terzan 5, 22 - 4U 1608-522, 23 - Aql X-1, 24 - 4U 2129+47, 25 - KS 1731-260.

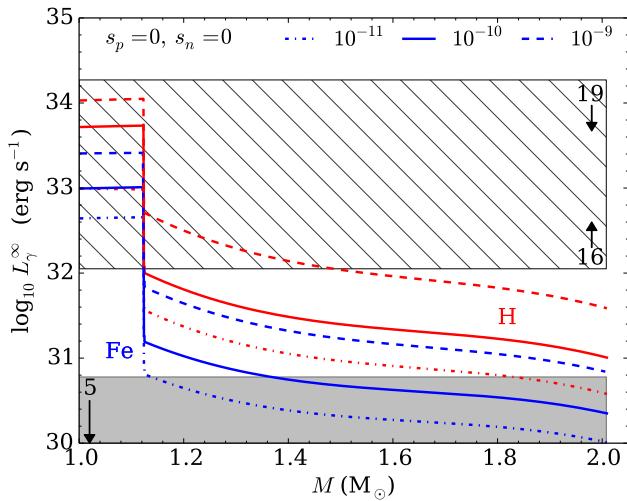


Figure 5. Surface photon luminosity L_γ^∞ versus mass M of a selection of qXRT for $\dot{M}/M_\odot = 10^{-(11,10,9)} \text{ yr}^{-1}$. Non-superfluid matter is considered ($s_p = 0$, $s_n = 0$), together with two envelope models: non-accreted (Fe) in blue and fully-accreted (H) in red. The hatched region indicates the range of luminosities covered by the objects 16, 17, 18, 19, 20, 22, 23 with relatively well determined accretion rate and luminosity. The grey strip corresponds to the low-luminosity object 5.

a higher amount of light elements have higher surface temperatures and thus surface photon luminosities. Hence models with a fully-accreted envelope will enter earlier the photon cooling stage and then cool faster than models with a non-accreted envelope. In the case of qXRT, at a given accretion rate models with a fully-accreted envelope have larger luminosities than the ones with a non-accreted envelope.

Thermal states of INS and qXRT obtained for non-superfluid matter with two limiting envelope models can explain almost all the observational data. Some objects like the INS 4 or the qXRT 12, 17, 19, 22, 23 require a fully-accreted envelope model and others, INS 17, 18, a non-accreted one. All the others are compatible with both envelope models. The INS 2 and 8 appear challenging for the model since they are hot (luminous) and young or middle-aged. Among the qXRT, the objects 16, 17, 18, 19, 20, 22, 23 are particularly interesting as their luminosity and accretion rate are rather well constrained, as well as the object 5, which has a well-constrained accretion rate and a very low luminosity.

In the case of non-superfluid matter, the DU threshold is a step-like function. Hence for $M < M_{\text{DU}}$ the DU process is turned off and for masses just above the threshold is turned on and fully operating. As a consequence, all 18 INS but the 2 too hot objects 2 and 8 would have masses between $1.0 M_\odot$ and $M_{\text{DU}} = 1.1 M_\odot$.

In Fig. 5, the relation between the NS mass and the luminosity of qXRT is plotted for three different accretion rates: $\dot{M}/M_\odot = 10^{-(11,10,9)} \text{ yr}^{-1}$ and the two envelope models. In addition the hatched region delimits the range of luminosities covered by the objects 16, 17, 18, 19, 20, 22, 23 with rather well-constrained

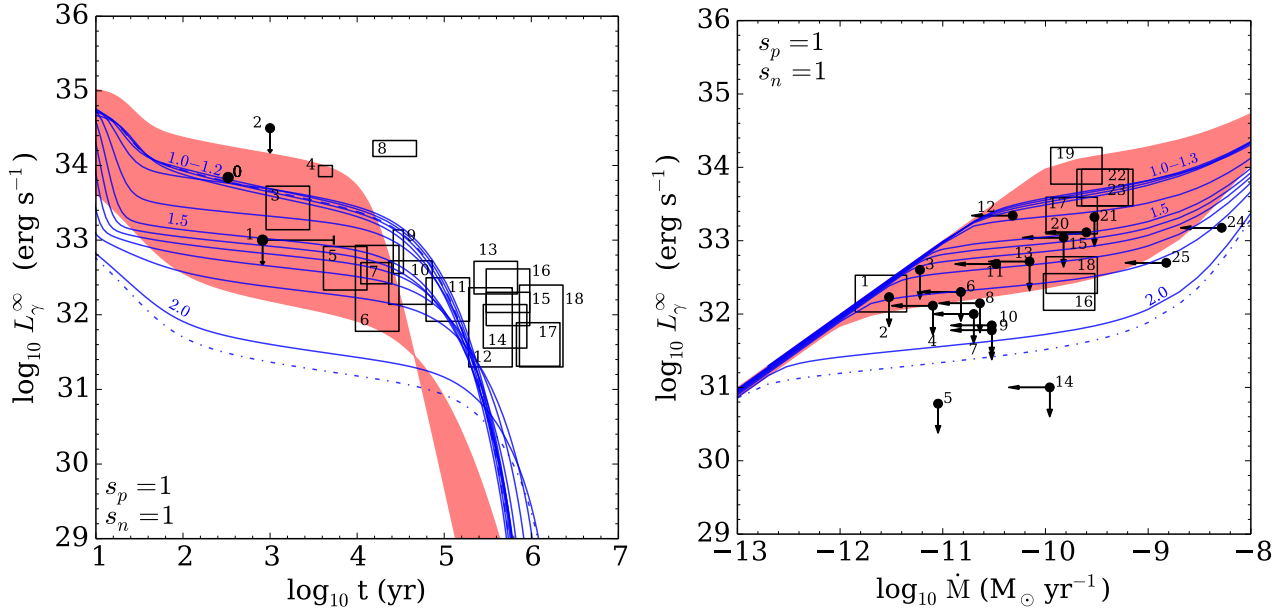


Figure 6. Thermal states of INS and NS in qXRT for superfluid NS matter with gaps calculated without including the effective mass effects: $s_p = 1$, $s_n = 1$.

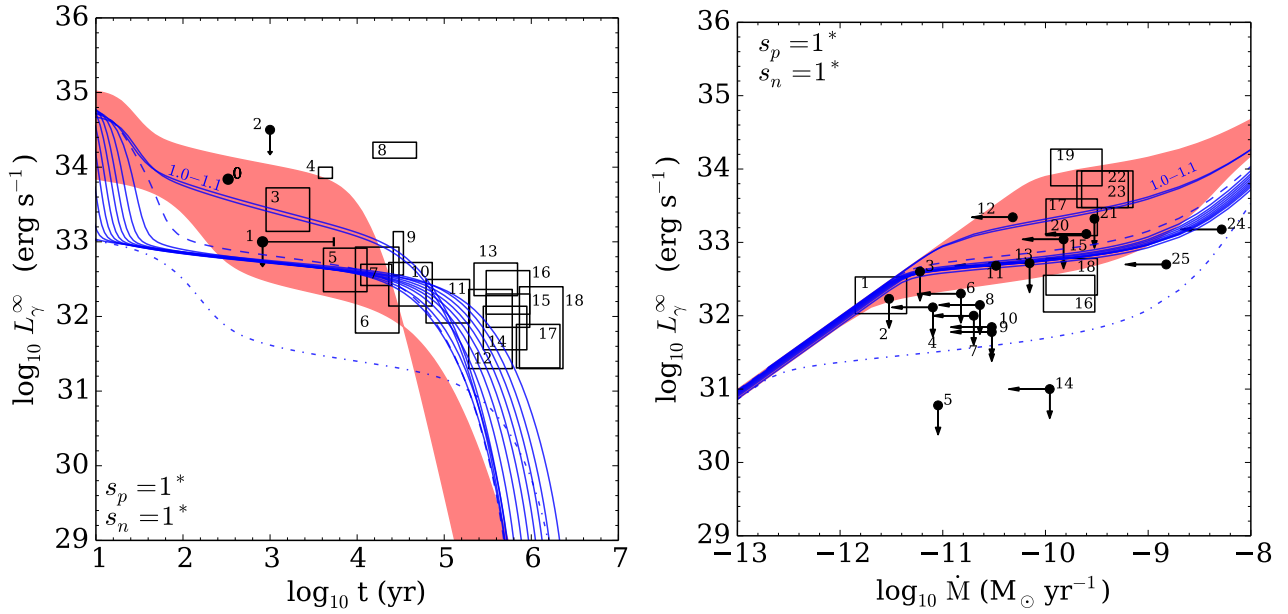


Figure 7. Thermal states of INS and NS in qXRT for superfluid NS matter with gaps calculated including the effective mass effects: $s_p = 1^*$, $s_n = 1^*$.

observational data and the grey area indicates the luminosity range of the least luminous object 5. The range of accretion rates has been chosen to cover the ones of all of these 8 objects. The figure indicates that while the qXRT 16, 17, 18, 19, 20, 22, 23 all have masses $M \simeq (1.0 - 1.1) M_\odot$, the object 5 requires larger neutrino losses and thus the DU process to be fully operating and the NS mass to be large enough in order to make the luminosity low enough. Thus while the DU process does not appear required to explain the thermal states of INS, the low-luminosity qXRT SAX J1808–3658 can only be explained if this efficient neutrino process is turned on already at not too low masses (to ensure a large enough region where the process is operating and thus producing sufficiently strong neutrino losses).

A striking feature of the relation $L_\gamma^\infty(M)$ in Fig. 5 is its step-like behavior, which is a direct consequence of the DU process having the same property. It implies that for a very wide range of luminosities $L_\gamma^\infty \sim (10^{31} - 10^{33}) \text{ erg s}^{-1}$, which is observationally relevant, NS have a unique mass $M \simeq M_{\text{DU}}$. In other words, the thermal states of low-mass NS (with $M < M_{\text{DU}}$) weakly depend on the NS mass. This feature appears difficult to reconcile with the current mass measurements (Lattimer 2012; Özel & Freire 2016) with masses ranging from ~ 1.0 to $2.0 M_\odot$, as also pointed out in Beznogov & Yakovlev (2015a) using a statistical approach to the INS and qXRT thermal states. A solution to this problem studied in Beznogov & Yakovlev (2015a,b) consists in broadening of the DU

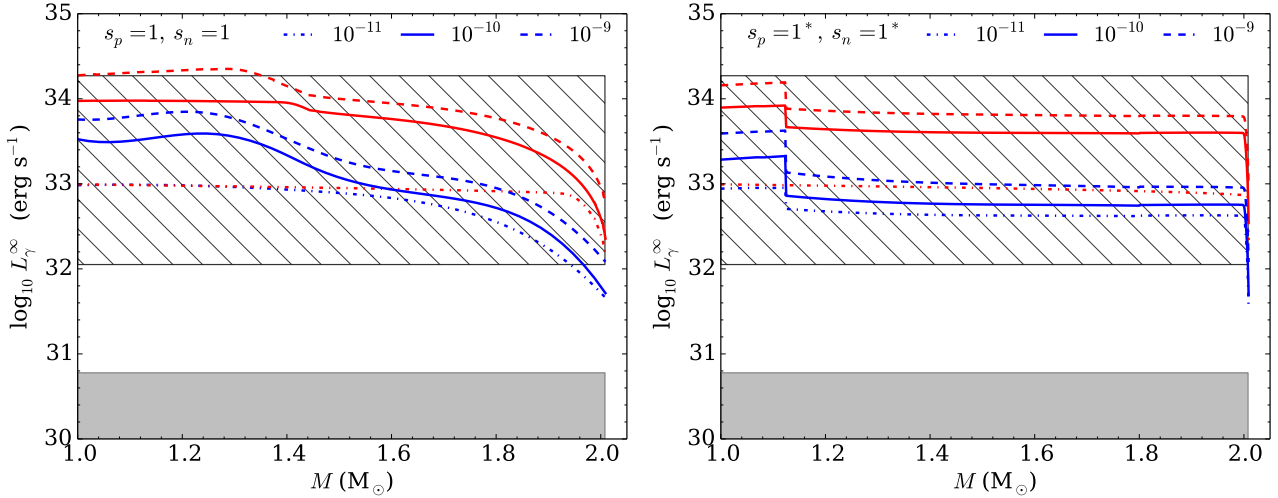


Figure 8. Surface photon luminosity L_γ^∞ versus mass M for a selection of qXRT. Model with superfluid gaps calculated without (with) effective mass effects on the left (right).

threshold, making it no longer a step-like function. In the following we study a possible origin of this broadening due to the inclusion of the proton and neutron superfluidity, based on our model of consistent EOS and superfluid gaps.

4.2 Consistent gaps and EOS

We now model the thermal states of INS and qXRT using an EOS and superfluid gaps that are consistently calculated. Cooling and heating curves are presented in Figs. 6 and 7, without and with effective mass effects included, $s_p = 1, s_n = 1$ and $s_p = 1^*, s_n = 1^*$, respectively, and the luminosity-mass relation for a selection of interesting qXRT is plotted in Fig. 8.

First, let us have a look at the thermal states of NS with $M < M_{\text{DU}}$, e.g., $M = 1.0 M_\odot$. As mentioned in Section 3.2, the effect of superfluidity is twofold. On one hand the specific heat and neutrino emissivity of processes to which the superfluid baryons contribute are strongly reduced when the temperature is smaller than the superfluid critical temperature. On the other hand, superfluidity triggers the additional n3P2 PBF process in the core, which compensates the effects of the superfluid reduction of the neutrino emissivity and specific heat. It should be noted that compared to previous works not including the anomalous contributions to the neutron PBF process, the reduction of the PBF neutrino emissivity by a factor four following Leinson (2016) reduces the neutrino losses and thus results in slightly larger luminosities.

All in all, in the absence of DU processes superfluidity accelerates the cooling of an INS (see, e.g., Page et al. 2004, 2009) while its temperature passes through the relevant critical temperature, resulting at later times in lower L_γ^∞ compared to the non-superfluid case, as can be seen in Figs. 6 and 7. Similarly the L_γ^∞ of qXRT with $M < M_{\text{DU}}$ is lower if superfluid effects are included, since the total neutrino losses are then larger due to the PBF processes. For the gaps used in this work the main effect of superfluidity on NS with $M > M_{\text{DU}}$ is the strong reduction of the DU process, as can be seen in Fig. 3, and thus a substantial reduction of the total neutrino emissivity. Hence INS and qXRT with a mass above the DU threshold have a higher L_γ^∞ compared to the non-superfluid case, and consequently the range of luminosities covered in the $L_\gamma^\infty - t$ and $L_\gamma^\infty - \dot{M}$ planes are much smaller.

When the effective mass effects are included, the critical temperature of the n3P2 superfluidity is larger at high densities $n_B \geq 0.7 \text{ fm}^{-3}$, i.e., $M > 1.7 M_\odot$, and thus the reduction of the DU process is larger for high masses, which results in higher values L_γ^∞ for both INS and qXRT compared to the case with $s_p = 1, s_n = 1$. However, for NS with masses $M < M_{\text{DU}}$, the PBF process is more powerful, since the leading neutrino process is the n3P2 PBF process, and since the critical temperature is smaller for $s_p = 1^*, s_n = 1^*$. This results in higher neutrino losses and thus lower L_γ^∞ compared to the case without effective mass effects on the superfluid gap. Hence the luminosity range of the cooling and heating curves for a given age or accretion rate, respectively, is smaller with the inclusion of the medium effects.

For superfluid NS, the additional source of neutrino losses due to the PBF process makes the transition to the photon cooling stage happen earlier compared to non-superfluid stars, and as a consequence these models cannot be reconciled with most if not all the old and yet luminous INS 13-18. In addition, the INS 4 can only marginally be explained if the medium effects are included. As shown in Fig. 8, none of the superfluid models is compatible with the qXRT 5, since the superfluid reduction of the DU process is too large. The models are however able to fit the thermal states of all the other qXRT, with the most luminous sources becoming consistent when covered with an envelope composed of light elements. The models with unscaled gaps also exhibit the property that L_γ^∞ is a smooth function of the mass, since the DU threshold is no longer a step-like function but a smooth one, see Fig 8. In other words, the problem exhibited by non-superfluid stars, that objects over a large range of luminosities have the same unique mass very close to M_{DU} , is solved by including superfluidity and the resulting smooth DU threshold.

Yet, the superfluid gaps consistent with the EOS are such that the thermal states of superfluid NS are not consistent with the observational data on INS (as already pointed out in Taranto et al. 2016) and even more on qXRT. Using the approach presented in this reference, we will in the following scale the superfluid gaps consistently calculated with the EOS and confront superfluid NS thermal states with the observational data.

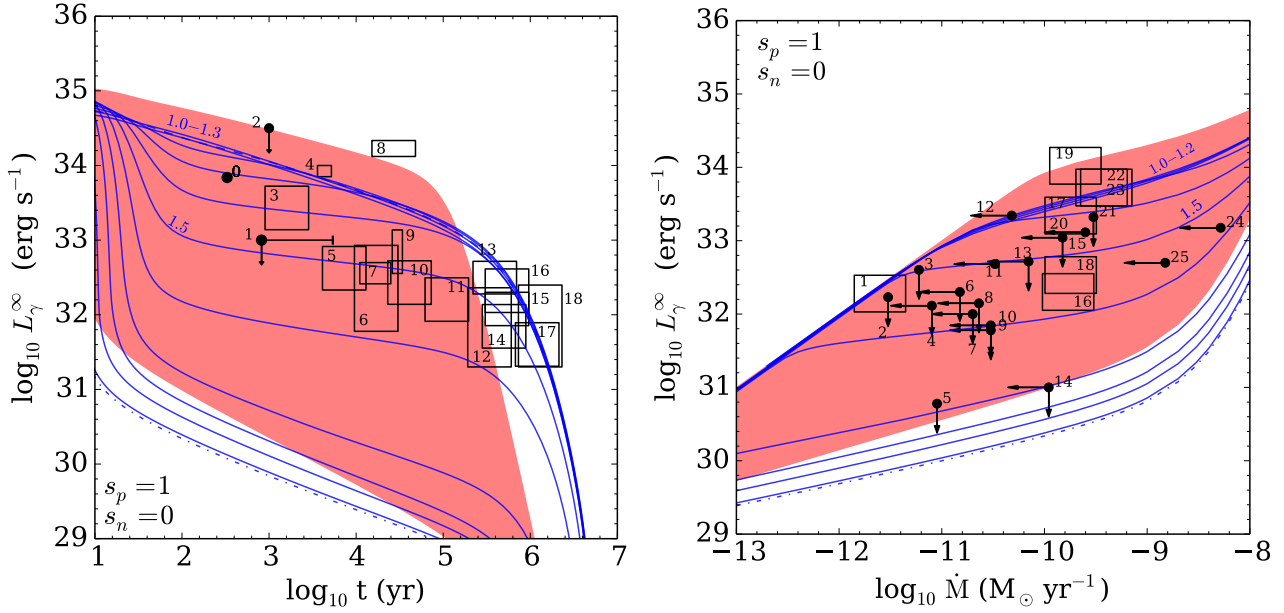


Figure 9. Same as Fig. 6 with unscaled proton superfluidity but no 3P2 neutron superfluidity: $s_p = 1$, $s_n = 0$.

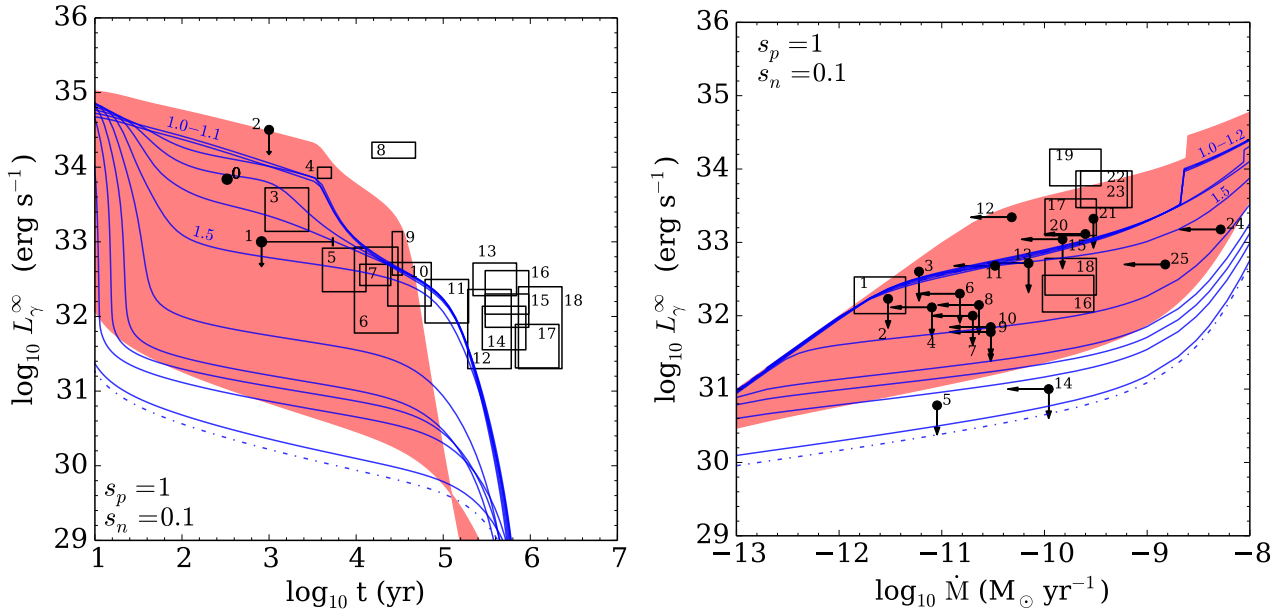


Figure 10. Same as Fig. 6 with unscaled proton superfluidity and scaled 3P2 neutron superfluidity: $s_p = 1$, $s_n = 0.1$.

4.3 Influence of neutron superfluidity

Let us now examine the influence of the n3P2 superfluidity, by scaling its critical temperature as a function of the density, while keeping the p1S0 gap unchanged. In the following only gaps not including the effective mass effects will be used.

First we consider the case of no superfluidity in the n3P2 channel, $s_n = 0$ and $s_p = 1$. Cooling and heating curves are presented in Fig. 9 and relations between the mass and luminosity for qXRT in Fig. 11 (left). Compared to the case with $s_n = 1$, $s_p = 1$, the absence of neutron superfluidity makes low-mass objects more luminous, as the efficient neutron PBF process is not triggered, and

massive stars become less luminous, since the DU process is not longer reduced for densities $n_B \gtrsim 0.7 \text{ fm}^{-3}$ or $M > 1.7 M_\odot$, as can also be seen in Fig. 3. The smooth DU threshold also makes the L_γ^∞ a smooth function of M , a given luminosity for a fixed accretion rate corresponding to a precise mass. The case $s_p = 1$, $s_n = 0$ is then consistent with all the observational data of INS and qXRT with a smooth mass distribution, except (albeit marginally) the hot middle-aged INS 8. In particular the low-luminous qXRT 5 is consistent with a massive NS with a non-accreted envelope or a NS with $M \approx M_{\text{max}}$ and a fully-accreted envelope.

Second, the n3P2 gap is taken to be the one obtained without medium effects, but scaled by a factor 0.1: $s_n = 0.1$ and $s_p = 1$.

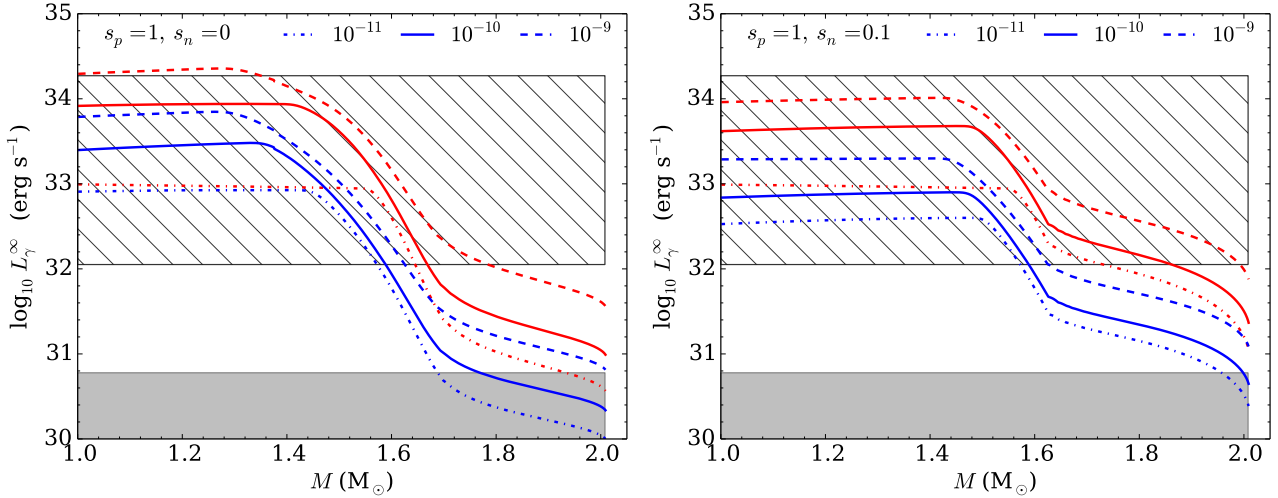


Figure 11. Same as Fig. 8 with unscaled proton superfluidity ($s_p = 1$) and scaled 3P2 neutron superfluidity: $s_n = 0$ (left) and $s_n = 0.1$ (right).

Thermal states of INS and qXRT and the luminosity for a set of qXRT are plotted as a function of the NS mass in Figs. 10 and 11 (right), respectively. When the temperature inside a cooling INS drops below the neutron critical temperature, or similarly, if the temperature inside a qXRT for which Eq. (17) is fulfilled is below T_c , then the neutron superfluid properties affect the thermal states, explaining the differences observed when comparing the models with $s_n = 0$ and $s_n = 0.1$, together with $s_p = 1$, for large ages and small accretion rates. Neutron superfluidity triggers the neutron PBF process, making low-mass INS and qXRT less luminous than in the case with $s_n = 0$. Thus INS 8 and 13 to 18 can not be explained. In order to explain these objects the neutron critical temperature should be even smaller or neutrons should not be superfluid at all at density $n_B \simeq (0.4 - 0.5) \text{ fm}^{-3}$ corresponding to NS masses larger than $1 M_\odot$. In addition, for $s_n = 0.1$ the DU process is always suppressed by superfluidity (see the DU threshold in Fig. 3) and high-mass INS and qXRT have a higher L_γ^∞ than those with no neutron superfluidity. Consequently, the qXRT 5 can only be interpreted as being a NS with $M \approx M_{\text{max}}$ with a fully-accreted envelope. Thanks to the smoothing of the DU threshold as observed in Fig. 3, $L_\gamma^\infty(M)$ is a smooth function as in the previous case.

4.4 Influence of proton superfluidity

Let us finally investigate the influence of the proton superfluidity on the thermal states of NS. We do not include neutron superfluidity ($s_n = 0$), as it has been shown to better reproduce the observational data in the previous section, and scale the proton superfluid gap with no effective mass effect by a factor 0.5, $s_p = 0.5$. Results are shown in Figs. 12 and 13.

Differences with the case $s_p = 1$ and $s_n = 0$ are very small and the model is consistent with all the observational data (marginally with the INS 8). The main effect of the reduced proton superfluidity is that the DU process is suppressed over a smaller range of densities than in the case with unscaled proton gap as shown in Fig. 3. This consequently makes the NS in which the DU process is turned on less luminous for a given mass (see, e.g., the cooling curve of $1.5 M_\odot$ NS in Figs. 9 and 12). Hence lower L_γ^∞ can be reached at lower mass when the proton superfluidity is reduced.

We also computed thermal states of NS for a model with a

proton superfluid gap scaled by a factor 0.5 and a neutron one taken unscaled, $s_p = 0.5$ and $s_n = 1$. Results are not shown, but thermal states of old INS with a high L_γ^∞ , objects 13 to 18, and of the low luminous qXRT 5 cannot be explained then because of the strong neutron PBF process and the reduction of the DU process at high density, respectively.

5 DISCUSSION AND CONCLUSIONS

In conclusion, for the BHF EOS with the DU process operating in all currently observed NS consistency with the thermal states of INS and NS in qXRT can be obtained if: (a) the neutrons are not superfluid or they are superfluid over a reduced range of densities corresponding to medium NS masses, i.e., in low-mass NS with $M < M_{\text{DU}}$ and early enough in massive stars; (b) the protons are superfluid (the precise magnitude of the gap being of little importance), but not in massive stars. No or little neutron superfluidity in low-mass stars together with proton superfluidity is required to slow down the cooling of middle-aged NS and thus to explain the thermal state of INS 8, XMMU J1731–347, as already pointed out in Ofengeim et al. (2015); Klochov et al. (2015), and of INS 13 to 18 and qXRT 19. Otherwise the triggering of the neutron PBF process or the non-superfluid reduction of the slow neutrino processes make the thermal states of low-mass NS inconsistent with these objects. In any case INS 8 and qXRT 19 (SAX J1750.8–2900) require a fully-accreted envelope, while INS 17 (PSR J2043+2740) and 18 (RX J0720.4–3125) a non-accreted one.

Both neutron and proton superfluidity have to be reduced early enough in massive stars in order to ensure that the DU process is fully operating so that the low luminosity of qXRT 5 (SAX J1808–3658) can be explained as being a NS with a high mass. The medium mass $M \lesssim 1.7 M_\odot$ derived for this object in Morsink & Leahy (2011) suggests that: a) the DU process is already operating in low-mass NS, as in our model, but reduced in such objects by baryon superfluidity, in order to reproduce the thermal state of XMMU J1731–347; b) that the baryon superfluidity is small in medium-mass NS $M \sim 1.4 M_\odot$ so that SAX J1808–3658 is consistently modelled.

All in all, as also stated in (Levenfish & Haensel 2007; Bezno-gov & Yakovlev 2015a; Han & Steiner 2017), qXRT sources require

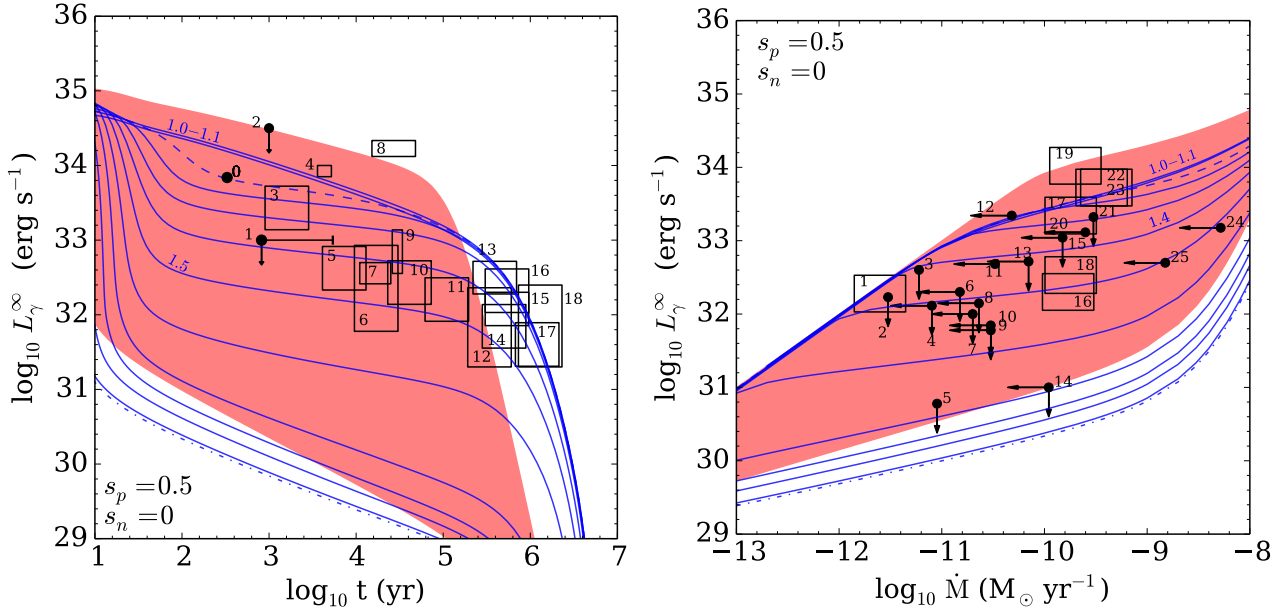


Figure 12. Same as Fig. 6 for no neutron superfluidity ($s_n = 0$) and a scaled ${}^1\text{S}_0$ proton superfluidity $s_p = 0.5$.

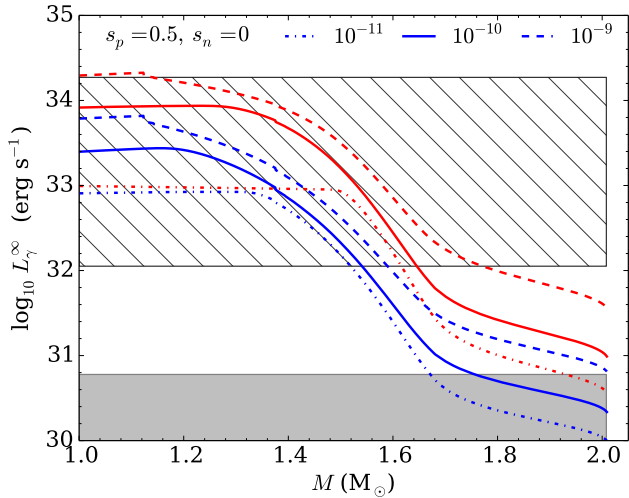


Figure 13. Same as Fig. 8 for no neutron superfluidity ($s_n = 0$) and a scaled ${}^1\text{S}_0$ proton superfluidity $s_p = 0.5$.

going beyond the so-called minimal cooling paradigm (Gusakov et al. 2004; Page et al. 2004, 2009), where all the necessary microphysical ingredients are included (in particular superfluidity), but fast cooling processes such as the DU process are not. Indeed even in case of strongly superfluid neutrons and protons, the neutrino losses due to the PBF processes are not large enough to explain the thermal state of qXRT 5, even more when taking into account the anomalous contributions to the PBF processes. Finally strong or moderate superfluidity for densities larger than the DU threshold appears required, so that the DU threshold is not a step-like function, but that the mass distribution of qXRT is smooth, ensuring that most NS do not have a mass close to M_{DU} .

It should be mentioned that the observational data we use in this work is subject to systematic and statistical errors. Two objects

are particularly constraining for our model: XMMU J1731–347 and SAX J1808–3658. Thus future observations may affect our conclusions regarding the density profiles of the neutron and proton superfluidity in the core. Yet we argue that the broadening of the DU threshold can be obtained by taking into account the baryon superfluid properties in the modeling of the thermal states of INS and qXRT, as was done in the present work. The so-called nuclear-medium modification of the thermal properties (Blaschke et al. 2013, 2004) can lead to a similar smoothing of the mass distribution [see also the discussion in Beznogov & Yakovlev (2015a,b)] and will be the topic of a future work.

There are equally successful cooling calculations based on very different nuclear EOSs and pairing gaps, but what we would like to point out is that even making some extreme (but theoretically justified and consistent) assumptions about the symmetry energy and cooling processes (DU active in all NS), our model cannot be falsified by the current data on NS cooling. Furthermore and more generally, in our work we used a minimal model of NS, assuming purely nucleon cores. We were able to obtain a reasonable agreement with existing observations. So for the time being, and in the context of observations of cooling INS and qXRT, there seems to be no urgent need to go beyond the minimal NS model, and to consider exotic NS cores (hyperons, quarks, boson condensates). This does not mean that the minimal model represents reality. In particular, if future theoretical calculations firmly demonstrate significant neutron pairing at high density, one might be required to abandon it.

ACKNOWLEDGEMENTS

This work was partially supported by the Polish NCN research grant OPUS6 no. 2013/11/B/ST9/04528. We also acknowledge partial support from the NewCompStar COST Action MP1304.

REFERENCES

- Aguilera D. N., Pons J. A., Miralles J. A., 2008, *A&A*, 486, 255
- Amundsen L., Østgaard E., 1985, *Nuclear Phys. A*, 442, 163
- Antoniadis J. et al., 2013, *Science*, 340, 448
- Baldo M., 1999, *Nuclear Methods And The Nuclear Equation Of State*, (Singapore:World Scientific)
- Baldo M., Cugnon J., Lejeune A., Lombardo U., 1992, *Nuclear Phys. A*, 536, 349
- Baldo M., Elgarøy Ø., Engvik L., Hjorth-Jensen M., Schulze H.-J., 1998, *Phys. Rev. C*, 58, 1921
- Baldo M., Schulze H.-J., 2007, *Phys. Rev. C*, 75, 025802
- Baldo M., Burgio G. F., Schulze H.-J., Taranto G., 2014, *Phys. Rev. C*, 89, 048801
- Beznogov M. V., Yakovlev D. G., 2015a, *MNRAS*, 447, 1598
- Beznogov M. V., Yakovlev D. G., 2015b, *MNRAS*, 452, 540
- Beznogov M. V., Fortin M., Haensel P., Yakovlev D. G., Zdunik J. L., 2016, *MNRAS*, 463, 1307
- Blaschke D., Grigorian H., Voskresensky D. N., 2004, *A&A*, 424, 979
- Blaschke D., Grigorian H., Voskresensky D. N., Weber F., 2012, *Phys. Rev. C*, 85, 022802(R)
- Blaschke D., Grigorian H., Voskresensky D. N., 2013, *Phys. Rev. C*, 88, 065805
- Burgio G. F., Schulze H.-J., Li A., 2011, *Phys. Rev. C*, 83, 025804
- Carlson J., Pandharipande V. R., Wiringa R., 1983, *Nuclear Phys. A*, 401, 59
- Ding D., Rios A., Dussan H., Dickhoff W. H., Witte S. J., Carbone A., Polls A., 2016, *Phys. Rev. C*, 94, 025802
- Elgarøy Ø., Engvik L., Hjorth-Jensen M., Osnes E., 1996, *Nuclear Phys. A*, 607, 425
- Elshamouty K. G. et al., 2013, *ApJ*, 777, 22
- Fonseca E. et al., 2016, *ApJ*, 832, 167
- Fortin M., Grill F., Margueron J., Page D., Sandulescu N., 2010, *Phys. Rev. C*, 82, 065804
- Fortin M. et al., 2016, *Phys. Rev. C*, 94, 035804
- Gandolfi S., Illarionov A. Y., Fantoni S., Pederiva F., Schmidt K. E., 2008, *Phys. Rev. Lett.*, 101, 132501
- Gusakov M. E., Kaminker A. D., Yakovlev D. G., Gnedin O. Y., 2004, *A&A*, 423, 1063
- Gusakov M. E., Kaminker A. D., Yakovlev D. G., Gnedin O. Y., 2005, *MNRAS* 363, 555
- Haensel P., Zdunik J. L., 1990a, *A&A*, 227, 131
- Haensel P., Zdunik J. L., 2003, *A&A*, 404, L33
- Haensel P., Potekhin A. Y., Yakovlev D. G., 2007a, *Neutron Stars 1. Equation of state and structure* (New York: Springer)
- Haensel P., Potekhin A. Y., Yakovlev D. G., 2007b, *Astrophysics and Space Science Library*, 326, Haensel
- Haensel P., Zdunik J. L., 2008, *A&A*, 480, 459
- Haensel P., Bejger M., Fortin M., Zdunik L., 2016, *European Physical Journal A*, 52, 59
- Han S., Steiner A. W., 2017, *Phys. Rev. C*, 96, 035802
- Heinke C. O., Jonker P. G., Wijnands R., Deloye C. J., Taam R. E., 2009, *ApJ*, 691, 1035
- Heney L. G., Forbes J. E., Gould N. L., 1964, *ApJ*, 139, 306
- Ho W. C. G., Elshamouty K. G., Heinke C. O., Potekhin A. Y., 2015, *Phys. Rev. C*, 91, 015806
- Khodel V. A., Khodel V. V., Clark J. W., 1998, *Phys. Rev. Lett.*, 81, 3828
- Khodel V. A., Clark J. W., Takano M., Zverev M. V., 2004, *Phys. Rev. Lett.*, 93, 151101
- Klochkov D. et al., 2015, *A&A*, 573, A53
- Lattimer J. M., Prakash M., Pethick C. J., Haensel P., 1991, *Phys. Rev. Lett.*, 66, 2701
- Lattimer J. M., 2012, *Annual Review of Nuclear and Particle Science*, 62, 485
- Leinson L. B., Perez A., 2006a, arXiv:astro-ph/0606653
- Leinson L. B., Pérez A., 2006b, *Phys. Lett. B*, 638, 114
- Leinson L. B., 2016, arXiv:1611.03794
- Levenfish K. P., Haensel P., 2007, *Ap&SS*, 308, 457
- Li Z. H., Lombardo U., Schulze H.-J., Zuo W., 2008, *Phys. Rev. C*, 77, 034316
- Lombardo U., Schulze H.-J., 2001, *Physics of Neutron Star Interiors*, Lecture Notes in Physics, 578, 30, Berlin Springer Verlag
- Morsink S. M., Leahy D. A., 2011, *ApJ*, 726, 56
- Ofengeim D. D., Kaminker A. D., Klochkov D., Suleimanov V., Yakovlev D. G., 2015, *MNRAS*, 454, 2668
- Özel F., Freire P., 2016, *ARA&A*, 54, 401
- Page D., Lattimer J. M., Prakash M., Steiner A. W., 2004, *ApJS*, 155, 623
- Page D., Lattimer J. M., Prakash M., Steiner A. W., 2009, *ApJ*, 707, 1131
- Page D., 2009, *Astrophysics and Space Science Library*, 357, 247
- Page D., Prakash M., Lattimer J. M., Steiner A. W., 2011, *Phys. Rev. Lett.*, 106, 081101
- Pons J. A., Miralles J. A., Geppert U., 2009, *A&A*, 496, 207
- Posselt B., Pavlov G. G., Suleimanov V., Kargaltsev O., 2013, *ApJ*, 779, 186
- Potekhin A. Y., Chabrier G., Yakovlev D. G., 1997, *A&A*, 323, 415
- Potekhin A. Y., Yakovlev D. G., Chabrier G., Gnedin O. Y., 2003, *ApJ*, 594, 404
- Pudliner B. S., Pandharipande V. R., Carlson J., Pieper S. C., Wiringa R. B., 1997, *Phys. Rev. C*, 56, 1720
- Schiavilla R., Pandharipande V. R., Wiringa R. B., 1986, *Nuclear Phys. A*, 449, 219
- Schwenk A., Friman B., 2004, *Phys. Rev. Lett.*, 92, 082501
- Sharma B. K., Centelles M., Viñas X., Baldo M., Burgio G. F., 2015, *A&A*, 584, A103
- Shternin P. S., Yakovlev D. G., Heinke C. O., Ho W. C. G., Patnaude D. J., 2011, *MNRAS*, 412, L108
- Takatsuka T., Tamagaki R., 1993, *Prog. Theor. Phys. Suppl.*, 112, 27
- Taranto G., Baldo M., Burgio G. F., 2013, *Phys. Rev. C*, 87, 045803
- Taranto G., Burgio G. F., Schulze H.-J., 2016, *MNRAS*, 456, 1451
- Wiringa R. B., Stoks V. G. J., Schiavilla R., 1995, *Phys. Rev. C*, 51, 38
- Yakovlev D. G., Levenfish K. P., Shibanov Y. A., 1999, *Physics Uspekhi*, 42, 737
- Yakovlev D. G., Kaminker A. D., Gnedin O. Y., Haensel P., 2001, *Phys. Rep.*, 354, 1
- Yakovlev D. G., Levenfish K. P., Haensel P., 2003, *A&A*, 407, 265
- Yakovlev D. G., Levenfish K. P., Potekhin A. Y., Gnedin O. Y., Chabrier G., 2004, *A&A*, 417, 169
- Yakovlev D. G., Pethick C. J., 2004, *ARA&A*, 42, 169
- Yakovlev D. G., Ho W. C. G., Shternin P. S., Heinke C. O., Potekhin A. Y., 2011, *MNRAS*, 411, 1977
- Zhou X.-R., Schulze H.-J., Zhao E.-G., Pan F., Draayer J. P., 2004, *Phys. Rev. C*, 70, 048802
- Zdunik J. L., Haensel P., 2011, *A&A*, 530, A137

This paper has been typeset from a $\text{\TeX}/\text{\LaTeX}$ file prepared by the author.